

Safety Analysis of Integrated Adaptive Cruise and Lane Keeping Control Using Multi-Modal Port-Hamiltonian Systems

Siyuan Dai^{a,*}, Xenofon Koutsoukos^a

^a *Vanderbilt University, Nashville, TN, USA, 37240*

Abstract

A modern vehicle can be viewed as a complex cyber-physical system (CPS) where the vehicle dynamics interact with the software control systems. Adaptive cruise control (ACC) and lane keeping control (LKC), in particular, are foundational features for semi-autonomous and autonomous driving. Safety analysis of such systems is extremely important for realizing vehicle autonomy. Ensuring safety in such complex CPS is very challenging, especially in the presence of interactions between multiple subsystems, nonlinearities, hybrid dynamics, and disturbances. This paper presents an approach for safety analysis of automotive control systems using multi-modal port-Hamiltonian systems. The approach uses the Hamiltonian function as a barrier between the energy levels of the safe and unsafe states and employs passivity to prove that trajectories cannot cross this barrier. The approach is applied to the safety analysis of a vehicle dynamics composed with ACC and LKC. The goal is to ensure that the host vehicle will not collide with a lead vehicle and will not skid off of the road. The control design is implemented and evaluated using a hardware-in-the-loop simulation platform. The experimental results demonstrate the safety analysis approach including the impact of implementation effects such as discretization and quantization.

*Corresponding author
Email addresses: siyuandai@gmail.com (Siyuan Dai),
xenofon.koutsoukos@vanderbilt.edu (Xenofon Koutsoukos)

Keywords: Passivity, safety analysis, port-Hamiltonian systems, automotive systems, discretization, quantization

1. Introduction

An autonomous or semi-autonomous vehicle is an example of a complex cyber-physical system (CPS) with behavior emerging from interaction between the physical dynamics and control systems controlling the speed and steering
5 of the vehicle [1]. An adaptive cruise control (ACC) system controls the speed of the vehicle, and can be viewed as a hybrid system operating in two modes, throttle control mode where the throttle angle is determined and brake control mode where the brake pressure is determined. A lane keeping control (LKC) system controls the angle of the steering wheel in order to maintain a desired
10 position on the road. Safety analysis of such systems is extremely important for realizing vehicle autonomy.

The design of the ACC and LKC systems must ensure that the host vehicle can drive safely. The appearance of a lead vehicle provides an additional constraint for the ACC in that the host vehicle must maintain a desired speed
15 depending on the behavior of the lead vehicle. A lead vehicle which suddenly decelerates may create a safety problem for the host vehicle. The ACC design on the host vehicle must guarantee that the distance between the lead and host vehicle stay above a minimum threshold. Turns and curves provide constraints for the LKC in that the host vehicle must maintain a position in the center of the
20 lane. Large road curvatures create skidding problems. The control design must guarantee that the lateral acceleration does not exceed a maximum threshold. The behavior of the vehicle is affected by interactions between the longitudinal and lateral dynamics that must be taken into consideration for analyzing safety. The challenge considered in this paper is to prove the safety of an integrated
25 ACC and LKC system despite the subsystem interactions, nonlinearities, hybrid dynamics, disturbances from the environment, and implementation effects.

The first contribution of this paper is an approach for safety analysis of

CPS such as automotive control systems. The dynamics of the vehicle and the control systems are described using multi-modal port-Hamiltonian systems (PHS). The approach characterizes the safe states of the system using a bounded from above energy level of the Hamiltonian function. Similarly, the unsafe states of the system are represented using a bounded from below energy level of the Hamiltonian function. Passivity is used to prove that as long as the safe and unsafe energy regions do not overlap, trajectories that begin within a lower energy level (safe states) cannot terminate within a higher energy level (unsafe states).

Although the approach can be applied to any system described as a multi-modal PHS, the paper focuses on its application to a vehicle equipped with ACC and LKC. We consider the interactions between the longitudinal dynamics, lateral dynamics, ACC, and LKC. We derive safety conditions for the ACC and LKC which ensure that the host vehicle does not collide with a lead vehicle and skid off of the road. We use the vehicle parameters, disturbances, and safety conditions to select control parameters so that the closed-loop system is safe.

In order to evaluate and validate the approach, the control design is implemented and tested in a hardware-in-the-loop (HIL) simulation platform. The HIL platform consists of multiple electronic control units (ECUs) communicating with a real-time simulation of the vehicle dynamics using the simulation tool CarSim [2]. The communication is realized using the time-triggered network TTEthernet [3]. A model-based design methodology is used to implement the control software. An important consideration is to analyze how implementation effects such as discretization and quantization affect safety. We present results obtained for various sampling rates using the HIL platform and we compare these results with continuous-time simulation results obtained using CarSim and Simulink [4]. Our HIL simulation results demonstrate that the system is safe under various scenarios with different behaviors for the lead vehicle, slope of the road, turns, and wind disturbances.

The rest of the paper is organized as follows. Section 2 presents the related work. Section 3 presents the energy-based safety analysis approach applied to

multi-modal PHS. Section 4 applies the safety analysis approach to a vehicle
60 dynamics model composed with ACC and LKC systems. Section 5 describes
the implementation of the control design in a HIL platform and the simulation
results that demonstrate the safety analysis approach. The paper is concluded
in Section 6.

2. Background and Related Work

65 As the number of control features added to automobiles increase, automotive
CPS become more complex and rigorous engineering methods are needed to
ensure safety [5]. Designing of ACC is especially challenging because of the
need to satisfy the requirements and constraints in the real world [6]. Safety
verification based on model predictive control methods for ACC design has
70 been presented in [7]. An approach based on formal methods for reachability
analysis in the presence of disturbances is presented in [8]. Computational tools
for safety control based on abstractions instead of detailed vehicle models in
order to simplify the computation of the reachable sets have been presented
in [9].

75 A method based on control barrier functions for safety analysis of ACC is
developed in [10]. The approach balances the objectives of maintaining a desired
host vehicle velocity and a relative distance greater than a minimum threshold.
The proposed approach in this paper uses barrier functions in a similar way,
but derives the functions based on the Hamiltonian of the PHS model.

80 2.1. Multi-Modal Port-Hamiltonian Systems

The theory of PHS is presented in detail in [11]. A PHS consists of a set
of ports (control, interaction, resistive, and storage) interconnected through a
power-conserving Dirac structure [12]. PHS have significant implications for
passivity, which has been studied extensively for control design and analysis of
85 nonlinear systems [13]. A key component of PHS is the Hamiltonian function,
which is derived from the equations of the storage elements of the system. PHS

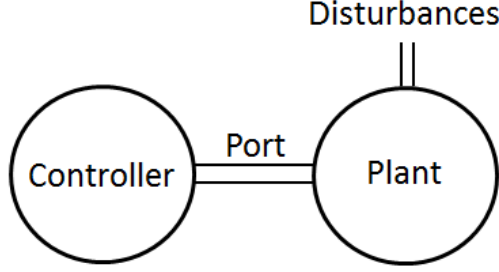


Figure 1: Generic plant system (with disturbances) and control system

can be used to describe hybrid systems using a framework known as multi-modal PHS [14].

Figure 1 provides a diagram of a generic multi-modal PHS composed of a
 90 plant connected to a controller via a power port that models the exchange of
 energy. The plant and the controller are, in general, multi-modal PHS and
 include disturbances from the environment that are shown as external power
 ports. Given a plant system with a Hamiltonian function $H_p(x_p)$, continuous
 states $x_p \in X_p \subseteq \mathbb{R}^{n_p}$, discrete states $s_p \in S_p$, disturbances $\delta \in \mathbb{R}^o$, and a
 95 control system a Hamiltonian function $H_c(x_c)$, continuous states $x_c \in X_c \subseteq \mathbb{R}^{n_c}$,
 and discrete states $s_c \in S_c$, where $\{n_p, n_c, o\} \subset \mathbb{N}$, we can write the set of
 dynamic equations of the closed-loop system as an input-state-output multi-
 modal PHS with Hamiltonian function $H(x) = H_p(x_p) + H_c(x_c)$, continuous
 states $x = \begin{bmatrix} x_p & x_c \end{bmatrix}^\top \in X = X_p \times X_c$, discrete states $s = \begin{bmatrix} s_p & s_c \end{bmatrix}^\top \in S =$
 100 $S_p \times S_c$, and initial states $X_0 = X_{p0} \times X_{c0} \times S_{p0} \times S_{c0}$. The discrete transitions
 are described by $(s, s') \in \mathbb{T} \subset S \times S$ and each transition is associated with a
 guard condition defined as $\text{Guard}(s, s') : \mathbb{T} \rightarrow 2^X$.

$$\begin{cases} \dot{x} &= [J(x, s) - R(x, s)] \frac{\partial H}{\partial x} + \begin{bmatrix} L_p(x_p, s_p) \\ 0 \end{bmatrix} \delta \\ \zeta &= \begin{bmatrix} L_p^\top(x_p, s_p) & 0 \end{bmatrix} \frac{\partial H}{\partial x} \end{cases} \quad (1)$$

$$J(x, s) = \begin{bmatrix} J_p(x_p, s_p) & -G_p(x_p, s_p)G_c^\top(x_c, s_c) \\ G_c(x_c, s_c)G_p^\top(x_p, s_p) & J_c(x_c, s_c) \end{bmatrix},$$

$$R(x, s) = \begin{bmatrix} R_p(x_p, s_p) & 0 \\ 0 & R_c(x_c, s_c) \end{bmatrix},$$

105 where $J_p(x_p, s_p) \in \mathbb{R}^{n_p \times n_p}$ and $J_c(x_c, s_c) \in \mathbb{R}^{n_c \times n_c}$ are skew-symmetric inter-connection matrices, $R_p(x_p, s_p) \in \mathbb{R}^{n_p \times n_p}$ and $R_c(x_c, s_c) \in \mathbb{R}^{n_c \times n_c}$ are symmetric positive semi-definite damping matrices, $G_p(x_p, s_p) \in \mathbb{R}^{n_p \times m}$, $G_c(x_c, s_c) \in \mathbb{R}^{n_c \times m}$, $L_p(x_p, s_p) \in \mathbb{R}^{n_p \times o}$, and (δ, ζ) are the input-output pairs corresponding to the disturbance port.

110 2.2. Canonical Coordinate Transform

The canonical coordinate transform method is used extensively in classical mechanics for analyzing the dynamical equations of physical systems [15]. These transformations preserve the Hamiltonian structure of the system and important system properties such as losslessness and passivity. Consider a PHS written in
115 input-state-output representation:

$$\begin{cases} \dot{x} &= [J(x) - R(x)] \frac{\partial H}{\partial x} + G(x)u \\ y &= G^\top(x) \frac{\partial H}{\partial x} \end{cases} \quad (2)$$

where $x \in \mathbb{R}^n$, $u \in \mathbb{R}^m$, $y \in \mathbb{R}^m$, $J(x) \in \mathbb{R}^{n \times n}$ is skew-symmetric, $R(x) \in \mathbb{R}^{n \times n}$ is positive symmetric, and $G(x) \in \mathbb{R}^{n \times m}$. Consider a time-invariant coordinate transformation defined by $\bar{x} = \Phi(x)$, then the dynamic equations can be written as

$$\begin{aligned} \dot{\bar{x}} &= \frac{\partial \Phi}{\partial x}^\top \dot{x} \\ &= \frac{\partial \Phi}{\partial x}^\top [J(x) - R(x)] \frac{\partial H}{\partial x} + \frac{\partial \Phi}{\partial x}^\top G(x)u \\ &= \frac{\partial \Phi}{\partial x}^\top [J(x) - R(x)] \frac{\partial \Phi}{\partial x} \frac{\partial H(\Phi^{-1}(\bar{x}))}{\partial \bar{x}} + \frac{\partial \Phi}{\partial x}^\top G(x)u \end{aligned} \quad (3)$$

120 and the output equation becomes

$$y = G^\top(x) \frac{\partial \Phi}{\partial x} \frac{\partial H(\Phi^{-1}(\bar{x}))}{\partial \bar{x}}.$$

The matrices $\frac{\partial \Phi}{\partial x}^\top J(x) \frac{\partial \Phi}{\partial x}$ and $\frac{\partial \Phi}{\partial x}^\top R(x) \frac{\partial \Phi}{\partial x}$ are skew-symmetric and positive symmetric, respectively, which means that the coordinate transformed system is also a PHS and the new Hamiltonian function is $H(\Phi^{-1}(\bar{x}))$. The canonical

coordinate transform is used in our work to show how the Hamiltonian function
125 can be used as a barrier function to ensure safety.

2.3. Barrier certificates

Barrier certificates, which are similar in structure to Lyapunov functions, are typically used for the purpose of analyzing nonlinear systems with uncertainties [16] including differential-algebraic systems with uncertain inputs [17].
130 Barrier certificates are functions which denote that there are no state trajectories starting from a given set of initial conditions that end up in an unsafe region [18].

Barrier certificates can be used to analyze safety of hybrid systems [19]. These barrier certificates are functions of both continuous and discrete states.
135 Computation of barrier certificates is challenging and computationally expensive [20]. If the dynamic equations of the system are described as polynomial functions, a sum of squares programming method can be used to approximate the barrier certificates by characterizing state regions as semi-algebraic sets and using semi-definite programming to obtain the optimal solution [21].

140 The approach presented in this paper is based on barrier certificates, using the Hamiltonian function as a barrier between safe and unsafe states. In contrast to a barrier certificate, the Hamiltonian function is derived directly from the model. Similar to safety analysis using barrier certificates, this paper shows that trajectories beginning from the safe region cannot reach the unsafe region.
145 However, the barrier certificate typically separates the initial and unsafe states using its zero level set, while the Hamiltonian function characterizes the initial and unsafe states using two energy levels. Passivity conditions can be used to prevent trajectories starting in the safe region from reaching the unsafe region.

3. Safety Analysis

150 We consider the plant and controller dynamics described by a multi-modal PHS. We characterize the initial and unsafe regions using the energy of the

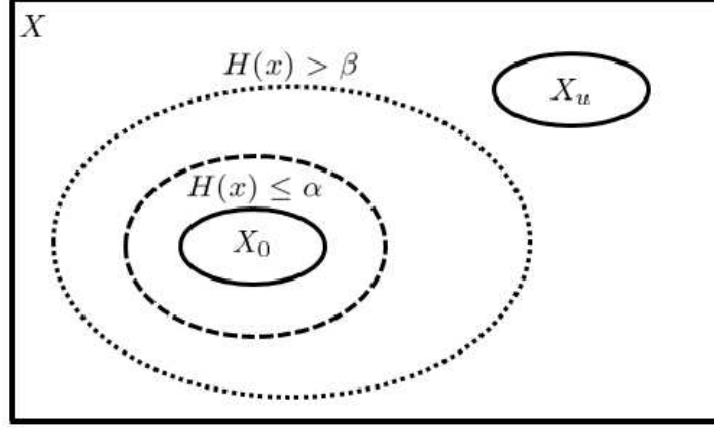


Figure 2: The Hamiltonian function prevents the trajectory from reaching the unsafe set X_u .

Hamiltonian function and show that the system trajectory cannot enter the unsafe region. Figure 2 illustrates the main idea of the safety analysis method. The method is based on using energy levels of the system as bounds in order to
 155 prove the safety. Given a multi-modal PHS represented as (1) with Hamiltonian function $H(x)$ and bounded disturbances, the safety problem is to show that there are no trajectories that reach an unsafe region of the state space.

Definition 1. *Given a multi-modal PHS (1) and $H(x)$ with continuous states $X = X_p \times X_c \subseteq \mathbb{R}^{n_p+n_c}$, discrete states $S = S_p \times S_c$, initial states $X_{p0} \times X_{c0} \times$
 160 $S_{p0} \times S_{c0} \subseteq X \times S$, unsafe states $X_{pu} \times X_{cu} \times S_{pu} \times S_{cu} \subseteq X \times S$, initial continuous states for each discrete state and disturbances $\Delta \subset \mathbb{R}^o$. For each discrete state $s \in S$, the initial continuous states are defined as $Init(s) = \{x \in X : (x, s) \in X_{p0} \times X_{c0} \times S_{p0} \times S_{c0}\}$ and the unsafe continuous states are defined as $Unsafe(s) = \{x \in X : (x, s) \in X_{pu} \times X_{cu} \times S_{pu} \times S_{cu}\}$. A system trajectory
 165 $\Gamma(x(t), s(t)) : [0, T] \rightarrow X \times S$ is unsafe if there exists a positive time instant T and a finite sequence of discrete transitions (s, s') at times $0 \leq t_1 \leq \dots \leq t_N \leq T$ such that $\Gamma(x(0), s(0)) \in Init(s)$ and $\Gamma(x(T), s(T)) \in Unsafe(s)$. The system is safe if there are no unsafe state trajectories.*

Theorem 1 describes the safety conditions:

170 **Theorem 1.** A multi-modal PHS described by (1) and $H(x)$, with continuous states $x \in X$, discrete states $s \in S$, initial states $\text{Init}(s)$, unsafe states $\text{Unsafe}(s)$, and bounded disturbances $\delta \in \Delta$ is safe if the canonical coordinate transformation $\bar{x} = \Phi(x)$ and transformed Hamiltonian function $H(\Phi^{-1}(\bar{x}))$ satisfy the following four conditions with $\alpha \leq \beta$

- 175
1. $H(\Phi^{-1}(\bar{x})) \leq \alpha, \forall x \in \text{Init}(s)$
 2. $H(\Phi^{-1}(\bar{x})) > \beta, \forall x \in \text{Unsafe}(s)$
 3. $\zeta^\top \delta \leq \frac{\partial H(\Phi^{-1}(\bar{x}))}{\partial \bar{x}}^\top \bar{R}(\bar{x}, s) \frac{\partial H(\Phi^{-1}(\bar{x}))}{\partial \bar{x}}, \forall \{x, \delta\} \in X \times \Delta$
 4. $H(\Phi^{-1}(\bar{x})) \leq \alpha, \forall (s, s')$

Proof. Suppose that the Hamiltonian function $H(x)$ satisfy the four conditions in Theorem 1, yet there exists a time $T \geq 0$, an input δ , and initial states $\text{Init}(s)$,
180 and a trajectory $\Gamma(x(t), s(t))$ such that $\Gamma(x(T), s(T)) \in \text{Unsafe}(s)$. We show that the Hamiltonian function cannot simultaneously satisfy the four conditions and reach the unsafe region, thus proving safety by contradiction. The time derivative of the Hamiltonian functions $\frac{dH}{dt}$ can be written as:

$$\begin{aligned}
 \frac{\partial H(x)}{\partial x}^\top \dot{x} &= \frac{\partial H(x)}{\partial x}^\top [J(x, s) - R(x, s)] \frac{\partial H(x)}{\partial x} + \frac{\partial H(x)}{\partial x}^\top L(x, s) \delta \\
 &= \frac{\partial H(\Phi^{-1}(\bar{x}))}{\partial \bar{x}}^\top [\bar{J}(\bar{x}, s) - \bar{R}(\bar{x}, s)] \frac{\partial H(\Phi^{-1}(\bar{x}))}{\partial \bar{x}} + \frac{\partial H(\Phi^{-1}(\bar{x}))}{\partial \bar{x}}^\top \bar{L}(\bar{x}, s) \delta \\
 &= -\frac{\partial H(\Phi^{-1}(\bar{x}))}{\partial \bar{x}}^\top \bar{R}(\bar{x}, s) \frac{\partial H(\Phi^{-1}(\bar{x}))}{\partial \bar{x}} + \zeta \delta
 \end{aligned}$$

185

$$\begin{aligned}
 \bar{J}(\bar{x}, s) &= \left. \frac{\partial \Phi}{\partial x} J(x, s) \frac{\partial \Phi}^\top \right|_{x=\Phi^{-1}(\bar{x})} \\
 \bar{R}(\bar{x}, s) &= \left. \frac{\partial \Phi}{\partial x} R(x, s) \frac{\partial \Phi}^\top \right|_{x=\Phi^{-1}(\bar{x})} \\
 \bar{L}(\bar{x}, s) &= \left. \frac{\partial \Phi}{\partial x} L(x, s) \right|_{x=\Phi^{-1}(\bar{x})}
 \end{aligned}$$

Condition (3) shows that the system trajectory on the time interval of $[0, T]$ is non-increasing, which indicates that $H(x(T)) \leq H(x(0))$. Additionally, condition (4) asserts that during a discrete transition, the Hamiltonian function
190 will not jump to an increasing value. These statements, however, contradict the original assumption that the system states start at $\text{Init}(s)$ and end at $\text{Unsafe}(s)$. As a result, we can conclude that the system is safe. \square

4. Collision and Skidding Avoidance

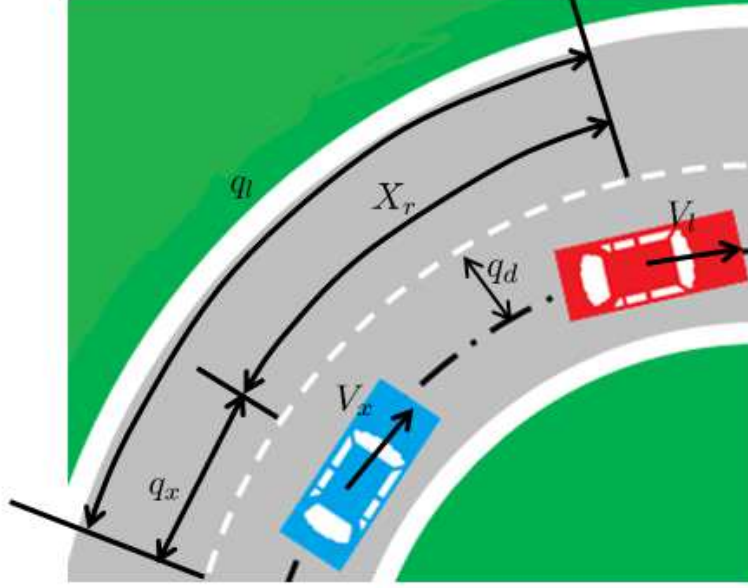


Figure 3: The host vehicle follows a lead vehicle on a curved road

195 In this section, we consider the safety problem of a vehicle equipped with both ACC and LKC following a lead car on a curved road (Figure 3). The host vehicle must maintain a safe distance between itself and the lead vehicle, and also maintain a safe lateral acceleration in order to not skid off the road. Of course, the lateral acceleration is affected by the interactions between the

200 lateral and longitudinal dynamics that need to be modeled. First, we model the longitudinal and lateral vehicle dynamics as PHS, including their interaction structure and disturbances. Then, we model the ACC and LKC systems as PHS and compose them with the vehicle dynamics. We use the Hamiltonian functions of all of the subsystems to derive the Hamiltonian function of the

205 closed-loop system. In the final step, we characterize the unsafe regions of the state space using the energy of the Hamiltonian and show that the host vehicle will not collide with the lead vehicle or skid off of the road.

4.1. Multi-Modal PHS Model

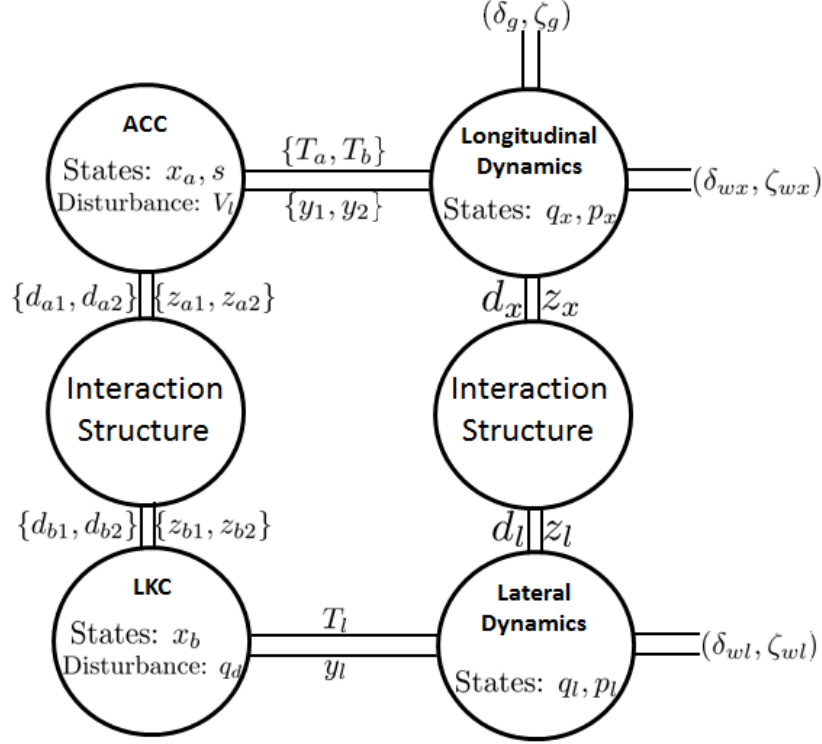


Figure 4: Closed-loop system

Figure 4 shows the multi-modal PHS of the vehicle dynamics connected
to the ACC and LKC systems via power ports. Disturbances from wind are
modeled as ports attached to the longitudinal and lateral dynamics, while the
disturbance due to the slope of the road is modeled as a port of the longitudinal
dynamics.

4.1.1. Longitudinal Dynamics

The longitudinal dynamics have state variables of longitudinal momentum
 p_x and longitudinal displacement q_x and two control ports (T_a, y_1) and (T_b, y_2) .
The longitudinal input force from the throttle, T_a , is a function of the throttle
valve angle θ_a , $T_a = C_a \theta_a$, where C_a is the experimental throttle constant.

The longitudinal input force from the brakes, T_b , is a function of the braking
 220 pressure P_b , $T_b = C_b P_b$, where C_b is the experimental braking constant. The
 outputs of the control ports y_1 and y_2 are the longitudinal speed V_x and $-V_x$,
 respectively. The longitudinal dynamics contain two disturbance ports whose
 inputs, δ_g and δ_{wx} are the disturbance forces resulting from the slope of the
 road and longitudinal wind, respectively. The outputs of the disturbance ports,
 225 ζ_g and ζ_{wx} , are the corresponding power conjugate values. The Hamiltonian
 function of the longitudinal dynamics is:

$$H_x(q_x, p_x) = \frac{1}{2m} p_x^2 + U_x(q_x),$$

where m represents the mass of the vehicle and $U_x(q_x)$ represents the potential
 energy. The longitudinal dynamics can be represented as a PHS with continuous
 states $\{q_x, p_x\} \in X_k \subseteq \mathbb{R}^2$, initial states $X_{k0} \subseteq X_k$, inputs $u_x = [T_a \ T_b]^\top$,
 230 and disturbances $d_x = [\delta_g \ \delta_{wx}]^\top$:

$$\left\{ \begin{array}{l} \begin{bmatrix} \dot{q}_x \\ \dot{p}_x \end{bmatrix} = \begin{bmatrix} 0 & 1 \\ -1 & -R_x \end{bmatrix} \begin{bmatrix} \frac{\partial H_x}{\partial q_x} \\ \frac{\partial H_x}{\partial p_x} \end{bmatrix} + \begin{bmatrix} 0 \\ G_x \end{bmatrix} u_x + \begin{bmatrix} 0 \\ 1 \end{bmatrix} d_x + \begin{bmatrix} \delta_g \\ \delta_{wx} \end{bmatrix} \\ y_x = \begin{bmatrix} 0 & G_x^\top \end{bmatrix} \begin{bmatrix} \frac{\partial H_x}{\partial q_x} \\ \frac{\partial H_x}{\partial p_x} \end{bmatrix}^\top \\ z_x = \begin{bmatrix} 0 & 1 \end{bmatrix} \begin{bmatrix} \frac{\partial H_x}{\partial q_x} \\ \frac{\partial H_x}{\partial p_x} \end{bmatrix}^\top \\ \begin{bmatrix} \zeta_g \\ \zeta_{wx} \end{bmatrix} = \begin{bmatrix} 0 & 1 \\ 0 & 1 \end{bmatrix} \begin{bmatrix} \frac{\partial H_x}{\partial q_x} \\ \frac{\partial H_x}{\partial p_x} \end{bmatrix}^\top \end{array} \right. \quad (4)$$

where $G_x = [1 \ -1]$, $R_x = a + \frac{bp_x}{m} + \frac{cm}{p_x}$, a represents the tire rolling friction
 constant, b represents the air resistance constant, c represents the static friction
 constant, and (d_x, z_x) represents the interaction port to the lateral dynamics.

4.1.2. Lateral Dynamics

235 The lateral dynamics have state variables $q_l = [q_y \ q_r]^\top$ and $p_l = [p_y \ p_r]^\top$,
 where p_y is the lateral momentum, p_r is the angular momentum, q_y is the lateral
 displacement, and q_r is the angular displacement. The lateral dynamics contain
 a control port (T_l, y_l) , where the output of the control port y_l is $V_y + l_f r$ (l_f

represents the length of the vehicle center to the front wheels). The lateral input
 240 force from the steering, T_l , is a function of the steering angle θ_s , $T_l = 2C_f\theta_s$,
 where C_f is the cornering stiffness of the front wheels. The lateral dynamics
 contains a disturbance port whose input, δ_{wy} , represents a disturbance force
 resulting from lateral wind. The output of the disturbance ports, ζ_{wy} , is the
 corresponding power conjugate value. The lateral velocity and yaw rate are
 245 represented by V_y , and r , respectively. The Hamiltonian function of the lateral
 dynamics is:

$$H_l(q_y, q_r, p_y, p_r) = \frac{1}{2m}p_y^2 + \frac{1}{2I}p_r^2 + U_l(q_y, q_r),$$

where I represents the moment of inertia of the vehicle and $U_l(q_y, q_r)$ represents
 the potential energy. The lateral dynamics can be represented as a PHS with
 continuous states $\{q_l, p_l\} \in X_l \subseteq \mathbb{R}^4$, initial states $X_{l0} \subseteq X_l$, input T_l , and
 250 disturbance δ_{wy} :

$$\begin{cases} \begin{bmatrix} \dot{q}_l \\ \dot{p}_l \end{bmatrix} = \begin{bmatrix} 0 & I \\ -I & -R_l \end{bmatrix} \begin{bmatrix} \frac{\partial H_l}{\partial q_l} \\ \frac{\partial H_l}{\partial p_l} \end{bmatrix} + \begin{bmatrix} 0 \\ G_l \end{bmatrix} T_l + \begin{bmatrix} 0 \\ K_l \end{bmatrix} d_l + \begin{bmatrix} 0 \\ L_l \end{bmatrix} \delta_{wl} \\ y_l = \begin{bmatrix} 0 & G_l^\top \end{bmatrix} \begin{bmatrix} \frac{\partial H_l}{\partial q_l} \\ \frac{\partial H_l}{\partial p_l} \end{bmatrix}^\top \\ z_l = \begin{bmatrix} 0 & K_l^\top \end{bmatrix} \begin{bmatrix} \frac{\partial H_l}{\partial q_l} \\ \frac{\partial H_l}{\partial p_l} \end{bmatrix}^\top \\ \zeta_{wl} = \begin{bmatrix} 0 & L_l^\top \end{bmatrix} \begin{bmatrix} \frac{\partial H_l}{\partial q_l} \\ \frac{\partial H_l}{\partial p_l} \end{bmatrix}^\top \end{cases} \quad (5)$$

$$R_l = \begin{bmatrix} \frac{W_1}{V_x} & \frac{W_2}{V_x} \\ \frac{W_2}{V_x} & \frac{W_3}{V_x} \end{bmatrix},$$

where $G_l = \begin{bmatrix} 1 & l_f \end{bmatrix}^\top$, $L_l = \begin{bmatrix} 1 & 0 \end{bmatrix}^\top$, and $K_l = \begin{bmatrix} 1 & 0 \end{bmatrix}^\top$. The parameters of R_l
 are $W_1 = 2C_f + 2C_r$, $W_2 = 2C_f l_f - 2C_r l_r$, and $W_3 = 2C_f l_f^2 + 2C_r l_r^2$, where C_r is
 the cornering stiffness of the rear wheels and l_r is the length of the vehicle center
 255 to the rear wheels, and (d_l, z_l) represents the interaction port to the longitudinal
 dynamics.

4.1.3. Interaction Between Longitudinal and Lateral Dynamics

Interactions between the longitudinal and lateral dynamics are a result of
 the vehicle heading angle being affected by the longitudinal velocity and can be

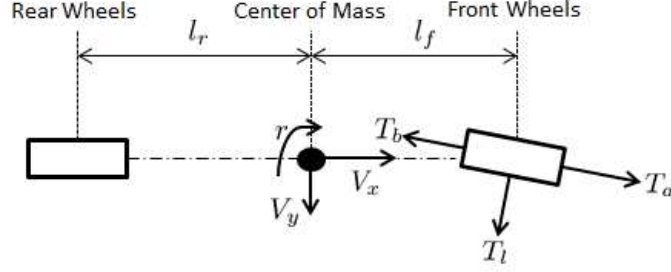


Figure 5: Free-body diagram of the vehicle dynamics

260 derived by analysis of the free-body diagram in Figure 5 [5]. The x-component of the lateral force affecting the longitudinal motion is represented by d_x and its power-conjugate velocity is represented by z_x . The y-component of the longitudinal force affecting the lateral motion is represented by d_l and its power-conjugate velocity is represented by z_l . The interaction between the longitudinal
 265 and lateral dynamics is a mapping of velocity to force, which indicates a gyrator relationship. The gyrator ratio has units of kg/s which is represented by multiplying the mass of the vehicle with the yaw rate. The interaction structure is modeled as a Dirac structure modulated by the yaw momentum p_r :

$$\begin{bmatrix} d_x \\ d_l \end{bmatrix} = \begin{bmatrix} 0 & -\frac{mp_r}{I} \\ \frac{mp_r}{I} & 0 \end{bmatrix} \begin{bmatrix} z_x \\ z_l \end{bmatrix}. \quad (6)$$

4.1.4. Adaptive Cruise Control Design

270 The ACC is connected to the longitudinal vehicle dynamics through the control ports for controlling T_a and T_b . The objective of the ACC is to maintain a desired speed depending on the lead vehicle velocity V_l , which is modeled as a disturbance. If a lead vehicle is not detected, the desired vehicle velocity is the driver's set speed which makes the system behave as a conventional cruise
 275 control system. Assuming that there is a lead vehicle, the host vehicle's radar system determines the speed of the lead vehicle and the displacement between

the vehicles.

$$\begin{aligned} X_r(t) &= \int_0^t (V_l - V_x) d\tau + X_r(0) \\ &= \int_0^t \left(V_l(\tau) - \frac{1}{m} p_x(\tau) \right) d\tau + X_r(0). \end{aligned}$$

The state variables of the ACC are derived using the lead vehicle velocity and the desired relative distance $X_d = hV_l + S_0$, where h is the time headway and S_0 is the static distance constant. We combine the state variables into a vector $x_a = \begin{bmatrix} x_{at} & x_{ab} \end{bmatrix}^T$, where $x_{at} = \int_0^t ((1 + 0.2 \frac{X_r - X_d}{X_d}) V_l - V_x) d\tau$ and $x_{ab} = \int_0^t (V_x - (1 + 0.2 \frac{X_r - X_d}{X_d}) V_l) d\tau$.

The ACC is a hybrid system with discrete modes that correspond to throttle control and brake control. Each mode is described using two binary variables $s_a = \{s_t, s_b\}$, where $s_t = 1$ when throttle control is active and $s_b = 1$ is when brake control is active. We assume that the throttle control and brake control modes cannot be active simultaneously. We also assume that the throttle control and brake control modes cannot be inactive simultaneously, in which case the vehicle is manually operated. The guards of the discrete transitions are defined in (7), where h_+ and h_- are hysteresis constants introduced to prevent the system from rapidly alternating between accelerating and decelerating:

$$(\{s_t, s_b\}, \{s'_t, s'_b\}) \begin{cases} = (\{0, 1\}, \{1, 0\}) & \text{if } (1 + 0.2 \frac{X_r - X_d}{X_d}) V_l - V_x \geq 0, X_r \geq h_+ X_d \\ = (\{1, 0\}, \{0, 1\}) & \text{if } (1 + 0.2 \frac{X_r - X_d}{X_d}) V_l - V_x < 0, X_r < h_- X_d \end{cases} \quad (7)$$

We design the ACC to have the following Hamiltonian function:

$$H_a(x_a, s) = \frac{1}{2} (k_{ti} x_{at}^2 + k_{bi} x_{ab}^2),$$

where k_{ti} and k_{bi} are the gains of the Hamiltonian. The ACC system has continuous states $x_a \in X_a \subseteq \mathbb{R}^2$, discrete states $s_a = \{s_t, s_b\} \in S_a$, initial states $X_{a0} \times S_{a0} \subseteq X_a \times S_a$, and transitions $(s_a, s'_a) \in \mathbb{T} \subset S_a \times S_a$ with guard conditions $\text{Guard}(s_a, s'_a) : \mathbb{T} \rightarrow 2^{X_a}$. Its input-state-output PHS is described by:

$$\begin{cases} \dot{x}_a &= -R_a \frac{\partial H_a}{\partial x_a} + G_a u_a \\ y_a &= G_a^T \frac{\partial H_a}{\partial x_a} + M_a u_a \end{cases} \quad (8)$$

where (u_a, y_a) are the input-output pairs corresponding to the control port. The parameter matrices are:

$$R_a = \begin{bmatrix} s_t k_t & 0 \\ 0 & s_b k_b \end{bmatrix}, G_a = \begin{bmatrix} s_t P & 0 \\ 0 & s_b \end{bmatrix}, M_a = \begin{bmatrix} s_t k_{td} & 0 \\ 0 & s_b k_{bd} \end{bmatrix}.$$

300 where k_t and k_{td} are throttle control gains, and k_b and k_{bd} are brake control gains. P is a mapping of the ratio of the acceleration force to V_x that is typically derived from the inverse engine map of the vehicle.

4.1.5. Lane Keeping Control Design

The LKC connects with the lateral vehicle dynamics via the control port
305 for controlling T_l . The objective of the LKC is to maintain a desired lateral displacement q_d . The LKC shares the control port with the lateral dynamics and its state variable $x_b = q_y - q_d$ is derived using the desired lateral displacement. We design the LKC to have the following Hamiltonian function:

$$H_b(x_b) = \frac{1}{2} k_{si} x_b^2,$$

where k_{si} is the gain of the Hamiltonian. The LKC system has continuous states
310 $x_b \in X_b \subseteq \mathbb{R}$ and initial states X_{b0} , with dynamic equations as an input-state-output PHS with direct-feedthrough:

$$\begin{cases} \dot{x}_b &= u_b \\ y_b &= \frac{\partial H_b}{\partial x_b} + k_{sd} u_b, \end{cases} \quad (9)$$

where (u_b, y_b) are the input-output pairs corresponding to the control port and k_{sd} is the gain associated with the steering control.

4.1.6. Interaction Between ACC and LKC

315 It can be seen from (4) and (5) that the inputs to the longitudinal dynamics (T_a and T_b) affect the lateral dynamics. Similarly, the input to the lateral dynamics (T_l) affects the longitudinal dynamics. We connect the ACC and LKC using an interaction structure, which alters (8) and (9), so that the state

variables and outputs of the speed control are affected by the state variable of
 320 the steering control, and vice versa.

$$\left\{ \begin{array}{l} \dot{x}_a = -R_a \frac{\partial H_a}{\partial x_a} + G_a y_x + K_{a1} d_{a1} \\ u_x = G_a^\top \frac{\partial H_a}{\partial x_a} + M_a y_x + K_{a2} d_{a2} \\ \begin{bmatrix} z_{a1} \\ z_{a2} \end{bmatrix} = \begin{bmatrix} K_{a1}^\top & 0 \\ 0 & K_{a2}^\top \end{bmatrix} \begin{bmatrix} \frac{\partial H_a}{\partial x_a} \\ y_x \end{bmatrix} \end{array} \right. \quad (10)$$

$$\left\{ \begin{array}{l} \dot{x}_b = y_l + d_{b1} \\ T_l = \frac{\partial H_b}{\partial x_b} + k_{sd} y_l + d_{b2} \\ \begin{bmatrix} z_{b1} \\ z_{b2} \end{bmatrix} = \begin{bmatrix} 1 & 0 \\ 0 & 1 \end{bmatrix} \begin{bmatrix} \frac{\partial H_b}{\partial x_b} \\ y_l \end{bmatrix} \end{array} \right. \quad (11)$$

The purpose of the interaction structure is to lower the speed of the vehicle
 in the event of a turn by transferring energy from the ACC to the LKC. The
 interaction structure of the control system is represented by the following Dirac
 325 structure:

$$\begin{bmatrix} d_{a1} \\ d_{a2} \\ d_{b1} \\ d_{b2} \end{bmatrix} = \begin{bmatrix} 0 & 0 & J_c & 0 \\ 0 & 0 & 0 & M_c \\ -J_c^\top & 0 & 0 & 0 \\ 0 & -M_c^\top & 0 & 0 \end{bmatrix} \begin{bmatrix} z_{a1} \\ z_{a2} \\ z_{b1} \\ z_{b2} \end{bmatrix}. \quad (12)$$

The parameters J_c and M_c define how the speed control and the steering control
 interact.

4.1.7. Closed-Loop System

The standard feedback interconnection of the longitudinal vehicle dynam-
 ics with the ACC system is described using the power-conserving intercon-
 330 nection $u_x = -y_a$ and $y_x = u_a$. The standard feedback interconnection of
 the lateral vehicle dynamics with the LKC system is described using a sim-
 ilar power-conserving interconnection $u_l = -y_b$ and $y_l = u_b$. In order to
 verify system safety, we must first derive the Hamiltonian function and dy-
 335 namic equations of the closed-loop system by combining (4), (5), (6), (10), (11),

and (12). In order to derive the closed-loop system, we define the variables $q = [q_x \ q_l]^\top$, $p = [p_x \ p_l]^\top$, $x = [x_{at} \ x_{ab} \ x_b]^\top$, $\delta = [\delta_g \ \delta_{wx} \ \delta_l]^\top$, and $\zeta = [\zeta_g \ \zeta_{wx} \ \zeta_l]^\top$. The closed-loop system has a Hamiltonian function $\tilde{H}(q, p, z) = H_x + H_l + H_a + H_b$, continuous states $\{q, p, x\} \in \tilde{X}$, discrete states $s_a \in S_a$, initial states $\tilde{X}_0 = \tilde{X}_{p0} \times \tilde{X}_{c0} \times S_a$, disturbances $\delta = \{\delta_g, \delta_{wx}, \delta_{wy}\} \in \Delta_g \times \Delta_{wx} \times \Delta_{wy}$, and transitions $(s_a, s'_a) \in \tilde{\mathbb{T}} \subset S_a \times S_a$ with assigned guard conditions $\overline{\text{Guard}}(s_a, s'_a) : \tilde{\mathbb{T}} \rightarrow 2^{\tilde{X}}$.

$$\begin{cases} \begin{bmatrix} \dot{q} \\ \dot{p} \\ \dot{x} \end{bmatrix} = \begin{bmatrix} 0 & I & 0 \\ -I & \tilde{J} - \tilde{R} & \tilde{K} \\ 0 & -\tilde{K}^\top & -\tilde{Q} \end{bmatrix} \begin{bmatrix} \frac{\partial \tilde{H}}{\partial q} \\ \frac{\partial \tilde{H}}{\partial p} \\ \frac{\partial \tilde{H}}{\partial x} \end{bmatrix} + \begin{bmatrix} 0 \\ \tilde{L} \\ 0 \end{bmatrix} \delta \\ \zeta = \begin{bmatrix} 0 & \tilde{L} & 0 \end{bmatrix} \begin{bmatrix} \frac{\partial \tilde{H}}{\partial q} & \frac{\partial \tilde{H}}{\partial p} & \frac{\partial \tilde{H}}{\partial x} \end{bmatrix}^\top \end{cases} \quad (13)$$

where \tilde{J} , \tilde{L} , \tilde{R} , \tilde{K} , and \tilde{Q} are defined as:

$$\begin{aligned} \tilde{J} &= \begin{bmatrix} 0 & \frac{mp_r}{I} - M_c & -l_f M_c \\ -\frac{mp_r}{I} + M_c & 0 & 0 \\ l_f M_c & 0 & 0 \end{bmatrix}, \\ \tilde{R} &= \begin{bmatrix} R_x + s_t k_{td} + s_b k_{bd} & 0 & 0 \\ 0 & \frac{mW_1}{p_x} + k_{sd} & \frac{mW_2}{p_x} + l_f k_{sd} \\ 0 & \frac{mW_2}{p_x} + l_f k_{sd} & \frac{mW_3}{p_x} + l_f^2 k_{sd} \end{bmatrix}, \\ \tilde{K} &= \begin{bmatrix} s_t P & s_b & 0 \\ 0 & 0 & -1 \\ 0 & 0 & -l_f \end{bmatrix}, \tilde{L} = \begin{bmatrix} 1 & 1 & 0 \\ 0 & 0 & 1 \\ 0 & 0 & 0 \end{bmatrix}, \tilde{Q} = \begin{bmatrix} s_t k_t & 0 & -J_c \\ 0 & s_b k_b & 0 \\ J_c & 0 & 0 \end{bmatrix}. \end{aligned}$$

4.2. Safety Problem

The control gains can be selected to stabilize the host vehicle velocity to $V_l + 0.2 \frac{(X_r - X_d)V_l}{X_d}$ and the lateral displacement to q_d [22]. However, stability does not imply safety and we need to show that the host vehicle behaves in a safe manner. We consider a scenario in which a lead vehicle appears in front

of the host vehicle driving slower than the host vehicle. If the ACC does not react accordingly and slow the host vehicle to a reasonable speed, a collision may occur. The safety condition for the longitudinal dynamics asserts that the relative distance between the two vehicles will never reach a minimum distance q_m . We do not consider the case in which a lead vehicle appears in front of the host vehicle driving faster than or equal to the host vehicle set speed because since the controller stabilizes the host vehicle velocity to the set speed indicating that the relative distance between the two vehicles will not be smaller than the initial relative distance.

We represent the set of unsafe host vehicle displacement as:

$$X_{ku} = \left\{ q_x \in \mathbb{R} : q_x \geq \int_0^t V_l d\tau + q_l(0) + q_m \right\}, \quad (14)$$

where $q_l(0)$ is the initial displacement value of the lead vehicle. The system is unsafe if the displacement of the host vehicle exceeds that of the lead vehicle plus q_m , which is indicative of an impending collision. The safety condition for the closed-loop system must ensure that there are not state trajectories that can reach the unsafe region described by (14).

Safety for the lateral acceleration depends on the interactions between the longitudinal and lateral dynamics. The inputs to the longitudinal dynamics (T_a and T_b) affect the lateral dynamics. Similarly, the input to the lateral dynamics (T_l) affects the longitudinal dynamics. In order for the vehicle to operate safely on the road, its lateral acceleration must not exceed a maximum value A_m . If the lateral acceleration exceeds A_m , the vehicle will skid. The lateral acceleration is affected by the yaw rate and longitudinal velocity of the vehicle. This interaction between lateral and longitudinal motion results in an unsafe region characterized as:

$$X_{lu} = \{p_x \in \mathbb{R}, p_r \in \mathbb{R} : p_x p_r \geq m^2 I A_m\}. \quad (15)$$

This safety condition indicates that longitudinal and lateral motion are bounded by a hyperbolic relationship. A large longitudinal momentum results in small

lateral and yaw momentum values, and vice versa. Therefore, we must verify that the product of longitudinal momentum and yaw rate does not exceed a maximum threshold. Given (13) and $\tilde{H}(q, p, z)$, the safety condition ensures
 380 that there are not trajectories that can reach the unsafe region described by (14) and (15).

4.3. Safety Analysis

A road can be divided into segments consisting of four types of road profiles: Straight road, decreasing curvature, constant curvature, and increasing curva-
 385 ture. For the straight segments, we only need to account for the longitudinal dynamics and the behavior of the lead vehicle because the lateral acceleration is effectively zero. In order to show safety, we make the following assumptions for the lead and host vehicle. The first assumption is that the initial velocity of the lead vehicle is less than a maximum velocity. The second assumption
 390 is that the initial relative distance between the vehicles is greater than a minimum distance. If the initial velocity of the vehicle is large compared to the host vehicle velocity, then the initial relative displacement can be low because the host vehicle does not need a large distance to react to the lead vehicle velocity. However, if the initial velocity of the vehicle is low compared to the host vehicle
 395 velocity, then the initial relative displacement must be high because the host vehicle needs a larger distance to react to the low lead vehicle velocity. The relationship between the initial relative distance and the initial vehicle velocities is described in (16).

$$X_r(0) = \frac{V_l^2(0)}{2a_l} - \frac{V_x^2(0)}{2\dot{V}_x}. \quad (16)$$

In order to safely navigate a curved section of the road, the vehicle must avoid
 400 the unsafe regions of X_{ku} and X_{lu} . Given a road curvature of ρ , the yaw momentum required is $p_r = \frac{I p_x}{m} \rho$, which shows the direct relationship between the yaw momentum and the longitudinal momentum. Additionally, the road curvature is related to the vehicle slip angle ω and steering angle θ_s :

$$\rho = \frac{\cos(\omega) \tan(\theta_s)}{l_f + l_r}, \omega = \arctan\left(\frac{l_r}{l_f + l_r} \tan(\theta_s)\right).$$

The lateral momentum depends on the longitudinal momentum, the yaw momentum, and the vehicle slip angle:

$$p_y = p_x \sin\left(\frac{p_r}{I} + \omega\right).$$

We need the following definitions for initial states, unsafe states, and guards. For each discrete state $s_a \in S_a$, the initial continuous states are defined as $\overline{\text{Init}}(s_a) = \{(q, p, x) \in \tilde{X} : (q, p, x, s_a) \in \tilde{X}_0\}$ and the unsafe continuous states are defined as $\overline{\text{Unsafe}}(s_a) = \{(q, p, x) \in \tilde{X} : (q_x, p_x, p_r) \in X_{ku} \times X_{lu}\}$. We restrict the system to having just two modes, throttle control mode or brake control mode. In the following analysis, we consider the following coordinate transformation $\tilde{\Phi}$ for the momentum variables [15].

$$\begin{bmatrix} \bar{p}_x \\ \bar{p}_y \\ \bar{p}_r \end{bmatrix} = \begin{bmatrix} \tilde{\Phi}_x(p_x) \\ \tilde{\Phi}_y(p_y) \\ \tilde{\Phi}_r(p_r) \end{bmatrix} = \begin{bmatrix} p_x - m(1 + 0.2 \frac{X_r - X_d}{X_d})V_l - M_c x_b \\ p_y + k_{si}(q_y - q_d) + M_c(x_{at} + x_{ab}) \\ p_r + k_{si}(q_r - \frac{q_d}{l_f}) + M_c \frac{x_{at} + x_{ab}}{l_f} \end{bmatrix}.$$

We apply Theorem 1 to the composed longitudinal dynamics, lateral dynamics, ACC, and LKC system. Given initial conditions $\overline{\text{Init}}(s_a)$, we derive the energy bound $\tilde{\alpha}$ as a function of the initial host vehicle velocity $V_x(0)$, initial relative distance $X_r(0)$, initial lead vehicle velocity $V_l(0)$, and initial road curvature $\rho(0)$. Consequently, we restate the first condition of Theorem 1 as $\tilde{H}(\tilde{\Phi}^{-1}(\bar{p})) \leq \tilde{\alpha}, \forall (q, p, x) \in \overline{\text{Init}}(s_a)$, where

$$\begin{aligned} \tilde{\alpha} = & m \frac{k_{td} + k_{bd}}{2} (V_x(0) - (1 + 0.2 \frac{X_r(0) - hV_l(0) - S_0}{hV_l(0) + S_0})V_l(0))^2 \\ & + \frac{m}{2} V_x^2(0) \sin^2(\rho(0)V_x(0) + \omega(0)) + \frac{I}{2} \rho^2(0) V_x^2(0). \end{aligned}$$

Given the unsafe states $\overline{\text{Unsafe}}(s_a)$, we derive the energy bound $\tilde{\beta}$ as a function of host vehicle velocity V_x , relative distance X_r , lead vehicle velocity V_l , and road curvature ρ . The energy of the transformed Hamiltonian function has a maximum value which indicates that the maximum lateral acceleration has been reached. Consequently, we restate the second condition of Theorem 1 as $\tilde{H}(\tilde{\Phi}^{-1}(\bar{p})) > \tilde{\beta}, \forall (q, p, x) \in \overline{\text{Unsafe}}(s_a)$, where

$$\begin{aligned} \tilde{\beta} = & m \frac{k_{td} + k_{bd}}{2} (V_x - 0.8V_l - \frac{M_c}{m}(q_y - q_d))^2 \\ & + \frac{m}{2} (V_x \sin(\rho V_x + \omega) + k_{si}(q_y - q_d))^2 + \frac{I}{2} (\rho V_x + k_{si}(q_y - \frac{q_d}{l_f}))^2. \end{aligned}$$

425 Given the disturbances $\{\delta_g, \delta_{wx}, \delta_{wy}\} \in \Delta$, we must guarantee that the system trajectory will never begin in $\overline{\text{Init}}(s_a)$ and end in $\overline{\text{Unsafe}}(s_a)$. Consequently, we restate the third condition of Theorem 1 as

$$\begin{aligned} \zeta_g \delta_g + \zeta_{wx} \delta_{wx} + \zeta_{wy} \delta_{wy} &\leq \frac{\partial \tilde{H}(\tilde{\Phi}^{-1}(\bar{p}))}{\partial(q, \bar{p})}^\top \frac{\partial \tilde{\Phi}}{\partial p} \tilde{R}(\tilde{\Phi}^{-1}(\bar{p})) \frac{\partial \tilde{\Phi}}{\partial p}^\top \frac{\partial \tilde{H}(\tilde{\Phi}^{-1}(\bar{p}))}{\partial(q, \bar{p})}, \\ &\forall(q, p, x, \delta_g, \delta_{wx}, \delta_{wy}) \in \tilde{X} \times \tilde{\Delta}. \end{aligned}$$

Discrete transitions between the throttle and brake control modes must also be taken into account in order to guarantee that the system will not transition
430 into $\overline{\text{Unsafe}}(s_a)$. Consequently, we restate the fourth condition of Theorem 1 as $\tilde{H}(\tilde{\Phi}^{-1}(\bar{p})) \leq \tilde{\alpha}, \forall(\{0, 1\}, \{1, 0\}) \cup (\{1, 0\}, \{0, 1\})$. In Section 5.5, the ACC and LKC are designed by selecting control parameters that satisfy these safety conditions.

5. Evaluation and Validation

435 Although continuous-time control design is useful for the early stages of design, evaluation and validation require implementation and deployment of the control system on a realistic computing platform. Since the safety approach is based on passivity and passivity may not be preserved because of discretization and quantization [23], this section presents an experimental evaluation and
440 validation of the integrated ACC and LKC using a hardware-in-the-loop (HIL) simulation platform. The main idea of the implementation is to "build enough passivity into the system" so that it will still be passive and safe after discretization and quantization.

5.1. Hardware-in-the-Loop Simulation Platform

445 Figure 6 shows the HIL simulation platform used for our experiments [24]. The vehicle dynamics are modeled in CarSim and the model is deployed and executed as a real-time process executing in a server with a real-time operating system (RT-Target in Figure 6.) The HIL platform has three ECUs which are connected to an 8-port 100Mbps TTEthernet switch from TTEch [3] to
450 form a time-triggered network. Each ECU is an IBX-530W box with an Intel

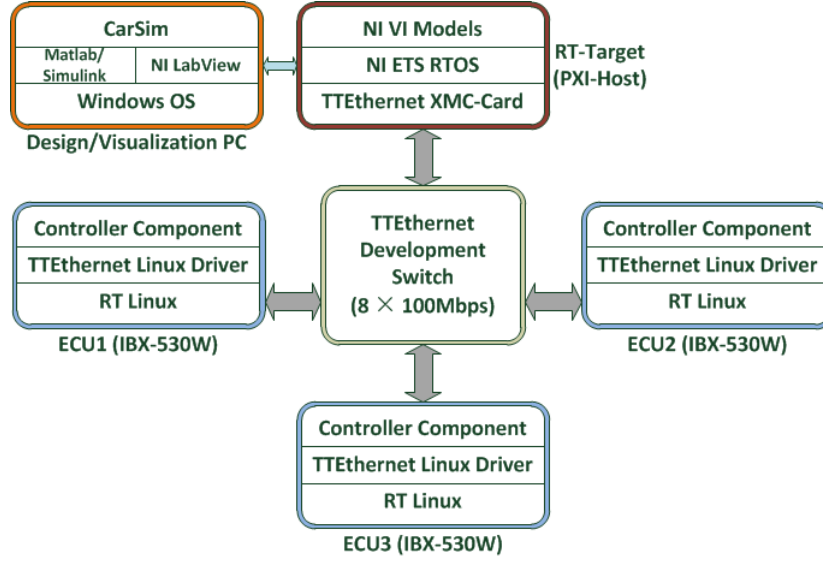


Figure 6: HIL simulator architecture [24]

Atom processor running a RT-Linux operating system and is integrated with a TTEthernet Linux driver, which is a software-based implementation of the TTEthernet protocol in order to enable communication with the other systems in a TTEthernet network. The RT-target is also connected to the time-triggered
455 networks using a TTEch PCIe-XMC card which enables the seamless integration and communication between the ECUs and the vehicle dynamics. The automotive control software is distributed over the ECUs and the tasks execute in the kernel space of RT-Linux which can utilize the synchronized time base off of the TTEthernet communication. The ACC and LKC are deployed
460 on ECU1 and communicate with the RT-Target via the TTEthernet network which provides a synchronized time base for computation and communication. The platform also employs two static schedule tables for executing the control tasks and communicating network messages [25].

5.2. Discretization

Initially, the continuous-time PHS is represented using block diagrams in a
465 continuous-time Simulink model. Transformation of the continuous-time model

into a discrete-time model is a procedure that involves bilinear transformations, up-samplers, and down-samplers [26]. State variables and subsequent computations inside the controllers are linked together through delays and adders. We
470 discretize the PHS controllers using sampling periods of 10 ms, 30 ms, and 50 ms.

Passivity is a property that degrades under discretization [23]. Intuitively, the larger the sampling period, the greater the degradation [27]. Further, even if the original continuous-time system is a passive PHS, its discretization is not
475 necessarily passive [28]. To circumvent this problem, we use the discretization approach developed in [29], in which the discrete-time output is modified as

$$y_d(k) = \frac{1}{t_s} \int_{kt_s}^{(k+1)t_s} y(t) dt.$$

This discretization approach guarantees that the resulting discrete-time system is passive. However, the approach requires a future output value of $y(t)$ at $(k+1)t_s$ which may not be possible to obtain especially if the system is highly
480 nonlinear. To address this problem, we discretize (13) using a sampling period that ensures the system satisfies the discrete-time passivity inequality:

$$t_s \sum_{k=0}^N u_d(k)^T y_d(k) \geq \mu_d t_s \sum_{k=0}^N \|u_d(k)\|^2 + \rho_d t_s \sum_{k=0}^N \|y_d(k)\|^2 \quad (17)$$

where N is a positive integer, μ_d is a real number, and ρ_d is a real number. In order to guarantee that the inequality in (17) is satisfied, we have to ensure that the sampling period is chosen so that the discrete-time passivity indexes are
485 larger than zero given $\mu_d = \mu - t_s \gamma - t_s \gamma \left| \rho \right| - t_s^2 \gamma^2 \left| \rho \right|$ and $\rho_d = \rho - t_s \gamma \left| \rho \right|$ [29].

5.3. Quantization

The ECUs that we use to implement the control system require 32-bit fixed-point data types. In Simulink the quantization process is done using MATLAB's Fixed-Point Toolbox, in which the word lengths for all data are set as fixdt(1,
490 32, 16) for 32-bit data types [4]. Simulink's quantizer is a uniform mid-tread quantizer, which is considered to be a passive quantizer where the input v and

output u mappings are bounded by two lines of slopes a and b , $av^2 \leq uv \leq bv^2$ [30]. However, even though the quantizer is passive does not necessarily mean that the quantized system is passive. In order to ensure passivity for the
495 quantized system, we implemented a passivity-preserving system introduced in [30]. It transforms the inputs and outputs of the quantized using a two-by-two transformation M , consisting of the values of $m_{11} = 2$, $m_{12} = -0.36$, $m_{21} = 0$, and $m_{22} = 1$, which are computed using the passivity indexes of the controllers.

500 This procedure involves the Simulink Coder (previously called Real-Time Workshop) which automatically generates the necessary C code using the the available bits in a word and the value ranges (Q format) [31]. The Simulink Coder generates code with proper computation according to the chosen fixdt. The code generated from the Simulink models is in C, which is compiled in order
505 to be deployed on the platform.

5.4. System Parameters

The proposed safety analysis is based on a PHS representation of the vehicle dynamics. Before the control implementation, it is necessary to identify the parameters in the PHS model and validate the analytical model. We use the
510 CarSim S-function of a mid-size sedan for performing the HIL simulations [2]. In order to validate the PHS representation of this model, we use passivity indexes that allow a way to characterize a system by determining its excess or shortage of passivity [32]. By selecting the model parameters so that the passivity indexes of the analytical model are similar to that of the CarSim model,
515 we can approximate the actual vehicle dynamics with an analytical model of a PHS.

The CarSim model has inherent bounds on its inputs [2]. The throttle angle valve (θ_f) has a lower bound of 0 rad and an upper bound of 1.5 rad. The brake pressure (P_b) has a lower bound of 0 and upper bound of 10 MPa. The steering
520 angle (δ) has a lower bound of -480 degrees and an upper bound of 480 degrees. Using these bounds, we derive that T_a has a lower bound of 0 N and an upper

bound of 3104 N, T_b has a lower bound of 0 N and an upper bound of 3715 N, and T_l has a lower bound of -1200 N and an upper bound of 1200 N.

Table 1: Table of vehicle parameter values

a	b	c	C_r	l_r	C_f	l_f
0.1	0.006	10	200	1.4	300	1.4

The model parameters for the vehicle model, shown in Table 1, are computed
525 so that the passivity indexes of the analytical model closely match that of the CarSim model. Evaluation of the passivity indexes is performed by executing both models through twenty diverse scenarios and optimizing the passivity indexes values using the method presented in [33]. In addition, according to the CarSim model, the vehicle has mass $m = 1650$ kg the inertia $I = 3234$ kg \cdot m².
530 Using the techniques demonstrated in [34], we determine that the passivity indexes of the CarSim model (ν_c, ρ_c) are (181, 0.6). We determined that the passivity indexes of the analytical model (ν_a, ρ_a) are (177, 0.6), indicating that the analytical model is a valid approximation of the CarSim model.

Passivity-based control is used to select the parameters of the ACC and
535 LKC by considering the total energy of the closed-loop system. Specifically, we consider the dissipation of the system being the difference between the stored energy and the incoming energy [35]. Using the experimental passivity index methods and the experimental data of the controllers, we compute the passivity indexes and L-2 gain of the controllers as $\mu = 0.8$, $\rho = 5.6$, and $\gamma = 2$. We find
540 that the discretized system will be passive given a sampling period smaller than $t_s \approx 65$ ms. The gain values of the controllers are verified to retain passivity given sampling periods of 10 ms, 30 ms, and 50 ms.

5.5. Simulation Results

In this section, we present the simulation results to illustrate the safety
545 analysis approach and to show that the system remains safe. Table 2 shows

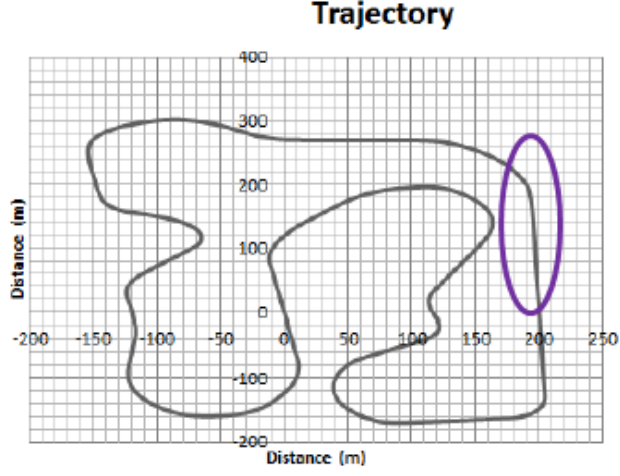


Figure 7: Road trajectory is shown in black; the purple circle shows the location of the vehicle during the simulation time of 80-90 seconds

the various scenarios that are used in the simulation. The trajectory shown in Figure 7 is encoded into the vehicle model in CarSim. The safety conditions derived in Section 4 are valid for vehicle velocities given a maximum road decline angle of 15 degrees which corresponds to $\delta_g = 4200$ N and a maximum lead vehicle deceleration of 5 m/s^2 which corresponds to a braking distance of 50 m
550 from 80 km/hr to 0 km/hr.

Simulation of the closed-loop system consists of two minutes of running time in which the host vehicle follows a lead vehicle on the road. As a baseline, we present simulation results obtained by integrating the CarSim model with a
555 continuous-time Simulink model of the ACC and LKC [36]. We generate results using the HIL simulation platform for sampling rates of 10, 30, and 50 ms (shown in the figures as the green, blue, and yellow lines) and we evaluate the safety (comparing with the safety bounds shown with the magenta lines) and the performance of the systems (comparing with the continuous-time results shown
560 with the red lines). Figure 8 shows the relative distance between the two vehicles for all the cases for the full two minutes of simulation time. Figure 9 shows the lateral acceleration of the host vehicles for all the cases for the full two minutes

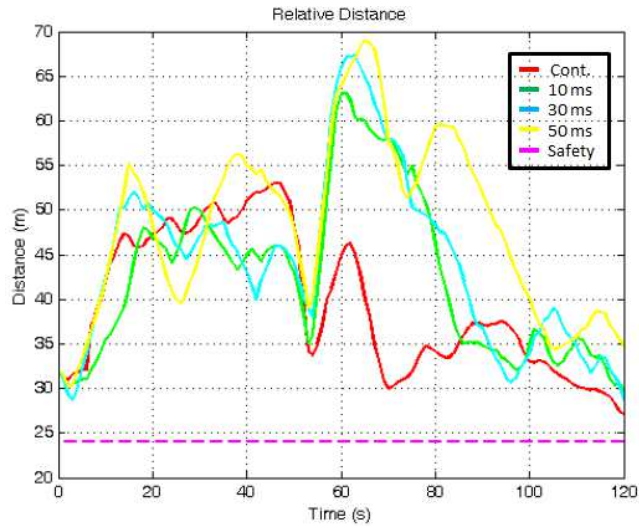


Figure 8: Relative distance for all cases

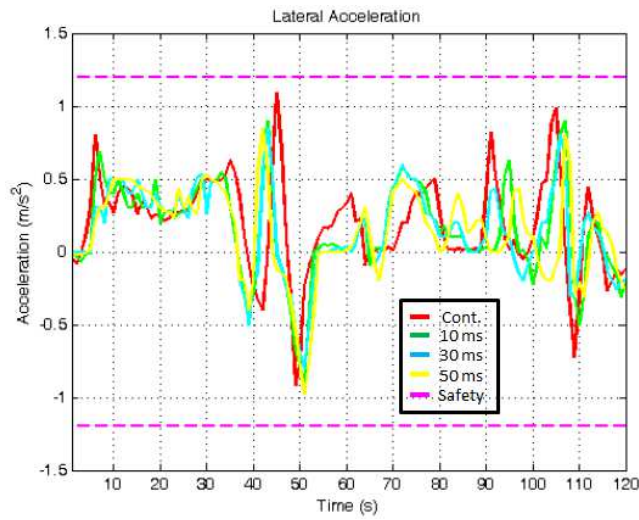


Figure 9: Lateral acceleration for all cases

Table 2: Table of simulation scenarios

Scenario	Time (s)	V_l (km/hr)	Slope ($^\circ$)	turns
1	0 – 40	65	0	3
2	40 – 52	65 – 77	0	1
3	52 – 60	77 – 85	–15	0
4	60 – 70	85	–15	1
5	70 – 90	85 – 50	–15	1
6	90 – 94	50	–15	0
7	94 – 103	50	0	1
8	103 – 120	50	15	1

Table 3: Table of controller gains

k_{ti}	k_{bi}	k_t	k_{td}	k_b	k_{bd}	k_{si}	k_{sd}
0.05	0.01	0.1	0.02	0.2	0.02	40	15

of simulation time. The results indicate that although all of the systems are safe, the discrete-time results are drastically different from the continuous-time results.

In order to compare the simulations results, we focus on the time between 80 and 90 seconds; it is shown on the highlighted circle in Figure 7. Figure 10 shows a comparison of the relative distance between the two vehicles under continuous-time and various sampling periods on the top left subplot and a comparison of the lateral acceleration of the host vehicle under continuous-time and various sampling periods on the bottom left subplot. The simulation results show that despite keeping to the objectives of speed and steering control, there is a noticeable difference between the different sampling periods; as the sampling period increases from 10 ms to 50 ms, the results for both the relative distance and the lateral acceleration shifts further away from the continuous-

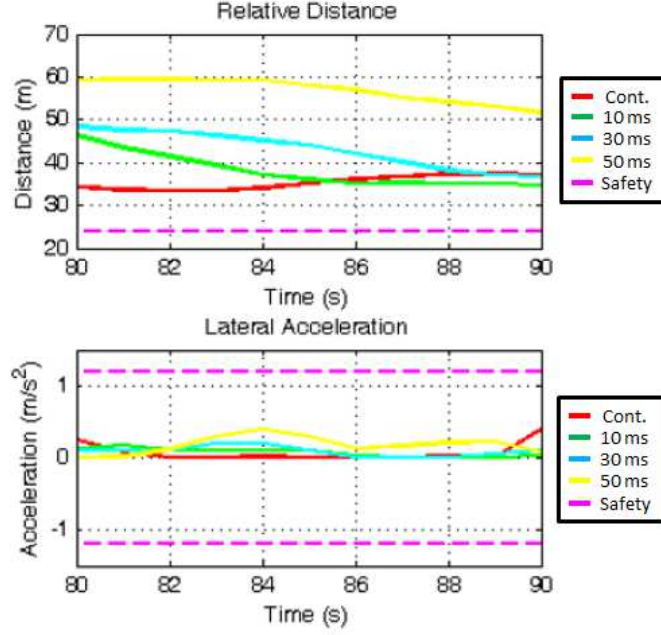


Figure 10: Relative distances and lateral accelerations between 80 - 90 s

time case. Even though all of the results are safe, the discrete-time results are noticeably different from the continuous-time results, which is attributed to the loss of passivity from discretization. The best performance is shown by the 10 ms results, which is reasonable because the sampling period is closest to continuous-time.

580

6. Conclusion

The approach in this paper addresses the safety problem for multi-modal PHS given complex interactions, nonlinearities, and hybrid dynamics. The approach ensures the safety of the system by characterizing safe and unsafe regions using energy levels of the Hamiltonian function and deriving conditions on model and control parameters. We demonstrate the approach by analyzing the safety conditions of an automotive control system to prevent collision and skidding. Simulation results from an automotive control system are recorded HIL plat-

585

form and show the effectiveness of the safety analysis approach. We conclude
 590 that even though the resulting discrete-time PHS is safe, there is a noticeable
 difference in performance compared to the continuous-time PHS, which is at-
 tributed to the loss of passivity during the discretization process. Future work
 could focus on an alternative discretization process for PHS which minimizes
 the loss of passivity during discretization.

595 References

- [1] J. Sztipanovits, X. Koutsoukos, G. Karsai, N. Kottenstette, P. Antsaklis,
 V. Gupta, B. Goodwine, J. Baras, S. Wang, Toward a science of cyber-
 physical system integration, *Proceedings of IEEE* 100 (2012) 29–44.
- [2] CarSim, <http://www.carsim.com>, Mechanical Simulation Corporation,
 600 Ann Arbor, MI, USA, 2013.
- [3] TTEthernet, <http://www.tttech.com/en/products/ttethernet/>, TTTech
 Computertechnik AG, Vienna, Austria, 2013.
- [4] MATLAB, Version R2012a, <http://www.mathworks.com>, The Mathworks,
 Inc., Natick, MA, USA, 2012.
- 605 [5] R. Rajamani, *Vehicle Dynamics and Control*, Springer, New York, NY,
 2006.
- [6] P. Nilsson, O. Hussien, A. Balkan, Y. Chen, A. D. Ames, J. W. Grizzle,
 N. Ozay, H. Peng, P. Tabuada, Correct-by-construction adaptive cruise con-
 trol: Two approaches, *IEEE Transactions on Control Systems Technology*
 24 (4) (2016) 1294–1307. doi:10.1109/TCST.2015.2501351.
 610
- [7] S. Li, K. Li, R. Rajamani, J. Wang, Model predictive multi-objective vehic-
 ular adaptive cruise control, *IEEE Transactions on Control System Tech-*
nologies 19 (2011) 556–566.

- [8] M. Althoff, D. Althoff, D. Wollherr, M. Buss, Safety verification of autonomous vehicles for coordinated evasive maneuvers, in IEEE Intelligent Vehicles Symposium (2010) 10781083.
- [9] M. R. Hafner, D. D. Vecchio, Computational tools for the safety control of a class of piecewise continuous systems with imperfect information on a partial order, SIAM Journal of Control Optimization 49 (2011) 24632493.
- [10] A. Ames, J. Grizzle, P. Tabuada, Control barrier function based quadratic programs with application to adaptive cruise control, in: Proceedings of the 53rd IEEE Conference of Decision and Control, Los Angeles, CA, USA, 2014.
- [11] V. Duindam, A. Macchelli, S. Stramigioli, H. Bruyninckx, Modeling and Control of Complex Physical Systems: The Port-Hamiltonian Approach, Springer, New York, NY, 2009.
- [12] A. van der Schaft, Port-hamiltonian systems: Network modeling and control of nonlinear physical systems, in: Advanced Dynamics and Control of Structures and Machines. CISM Courses and Lectures No. 444, CISM International Centre for Mechanical Sciences, Springer, New York, NY, USA, 2004, pp. 127–168.
- [13] H. Khalil, Nonlinear Systems, 3rd Edition, Prentice Hall, Upper Saddle River, NJ, 2002.
- [14] A. van der Schaft, Port-hamiltonian systems: An introductory survey, Proceedings of the International Congress of Mathematicians.
- [15] K. Fujimoto, T. Sugie, Canonical transformation and stabilization of generalized hamiltonian systems, Systems and Control Letters 42 (2001) 217–227.
- [16] S. Prajna, Barrier certificates for nonlinear model validation, Automatica 42 (2006) 117–126.

- [17] C. Sloth, G. Pappas, R. Wisniewski, Compositional safety analysis using barrier certificates, in: Hybrid System Computation and Control, Beijing, China, 2012.
- [18] S. Prajna, A. Rantzer, Primal-dual tests for safety and reachability, in: Hybrid Systems Computation and Control, Springer-Verlag, Zurich, Switzerland, 2005, pp. 542–556.
- [19] S. Prajna, A. Jadbabaie, Safety verification of hybrid systems using barrier certificates, in: Hybrid Systems Computation and Control, Springer-Verlag, Philadelphia, PA, USA, 2004, pp. 477–492.
- [20] S. Prajna, A. Jadbabaie, G. Pappas, A framework for worst-case and stochastic safety verification using barrier certificates, IEEE Transactions on Automatic Control 52 (8) (2007) 1415–1428.
- [21] S. Prajna, A. Papachristodoulou, P. Parrilo, Introducing sostools: A general purpose sum of squares programming solver, in: Proceedings of the IEEE Conference on Decision and Control, Las Vegas, NV, USA, 2002.
- [22] S. Dai, X. Koutsoukos, Model-based automotive control design using port-hamiltonian systems, in: International Conference on Complex Systems Engineering, Storrs, CT, USA, 2015.
- [23] C. Byrnes, W. Lin, Losslessness, feedback equivalence, and the global stabilization of discrete-time nonlinear systems, IEEE Transactions on Automatic Control 39 (1994) 83–98.
- [24] E. Eyisi, Z. Zhang, X. Koutsoukos, J. Porter, G. Karsai, J. Sztipanovits, Model-based control design and integration of cyberphysical system: An adaptive cruise control case study, Journal of Control Science and Engineering, Special Issue on Embedded Model-Based Control.
- [25] J. Porter, G. Karsai, J. Sztipanovits, Towards a time-triggered schedule calculation tool to support model-based embedded software design, in: Pro-

ceedings of the Seventh ACM International Conference on Embedded Software, EMSOFT '09, 2009, pp. 167–176.

- 670 [26] N. Kottenstette, J. Hall, X. Koutsoukos, J. Sztipanovits, P. Antsaklis, Design of networked control systems using passivity, *IEEE Transactions on Control Systems Technology* 21 (3) (2013) 649–665.
- [27] Y. Oishi, Passivity degradation under the discretization with the zero-order hold and the ideal sampler, 49th IEEE Conference on Decision and Control.
- 675 [28] S. Stramigioli, C. Secchi, A. J. van der Schaft, C. Fantuzzi, Sampled data systems passivity and discrete port-hamiltonian systems, *IEEE Transactions on Robotics* 21 (4) (2005) 574–587.
- [29] R. Costa-Castello, E. Fossas, On preserving passivity in sampled-data linear systems, *Proceedings of the 2006 American Control Conference* (2006) 4373–4378.
- 680 [30] F. Zhu, H. Yu, M. J. McCourt, P. J. Antsaklis, Passivity and stability of switched systems under quantization, *Conference on Hybrid Systems Computation and Control*.
- [31] K. K. Jiyang, K. Kum, J. Kang, S. W., A floating-point to fixed-point converter for fixed-point digital signal processors, *Second SUIF Compiler Workshop*.
- 685 [32] H. Yu, P. Antsaklis, A passivity measure of systems in cascade based on passivity indices, 49th IEEE Conference on Decision and Control.
- [33] R. Hooke, T. Jeeves, Direct search solution of numerical and statistical problems, *Journal of the Association of Computing Machinery* 7 (1969) 212–229.
- 690 [34] P. Wu, M. McCourt, P. Antsaklis, Experimentally determining passivity indices: Theory and simulation, in: *ISIS Technical Report ISIS-2013-002*, University of Notre Dame, 2013.

- 695 [35] R. Ortega, A. van der Schaft, F. Castanos, A. Astolfi, Control by intercon-
nection and standard passivity-based control of port-hamiltonian systems,
IEEE Transactions on Automatic Control 53.
- [36] S. Dai, X. Koutsoukos, Safety analysis of automotive control systems using
multi-modal port-hamiltonian systems, 19th ACM International Confer-
700 ence on Hybrid Systems: Computation and Control (HSCC 2016).